

Reactive Pore Expansion During Ammonia Vapor Post-Treatment of Ordered Mesoporous Silica Prepared with Mixed Glucopyranoside and Cationic Surfactants

Rong Xing and Stephen E. Rankin*

Chemical and Materials Engineering Department, University of Kentucky, 177 Anderson Hall,
Lexington, KY 40506-0046, U.S.A.

* To whom correspondence should be addressed. Fax: +1 859 323 1929; Tel: +1 859 257 9799;

E-mail: srankin@engr.uky.edu.

Abstract

n-octyl- β -D-glucopyranoside (C_8G_1) has the potential to serve as a functional, nonionic template for mesoporous oxides, but its use has been limited due to its propensity to form lamellar mesostructures. Here, 2D hexagonal-structured mesoporous silicas with variable pore sizes are synthesized with C_8G_1 by the “nanocasting” technique (polycondensation of tetramethoxysilane in concentrated acidic solutions with evaporation) by mixing it with cetyltrimethylammonium bromide (CTAB) to promote ordering. In an effort to stabilize the silica network structure, a mild treatment with ammonia vapor at 50 °C is introduced. Without ammonia treatment, the pore diameter remains constant as the C_8G_1 : CTAB weight ratio increases even up to 0.3: 1. When the as-made materials are treated with ammonia vapor, the degree of long-range order of the samples increases, and pore expansion is observed which increases in magnitude as the C_8G_1 content increases. Large degrees of expansion increase pore size fluctuations but do not eliminate long-range order. Materials with well-ordered, uniform pores can be made with C_8G_1 /CTAB mixtures by limiting the amount of ammonia or increasing the amount of silica precursor. A mechanistic study suggests that micelle swelling occurs with CTAB, but is limited by increased polycondensation of silica and favorable headgroup-silica interactions. With the

glucopyranoside surfactant, the extent of expansion is greater not only because of a change in the physical interaction with silica, but also because the Maillard reaction occurs under surprisingly mild conditions.

Keywords: nanocasting, templating, self-assembly, processing, expansion

Introduction

The synthesis of ordered mesoporous metal oxides using surfactant templating was first reported by Beck, Kresge, and coworkers in 1992.[1,2] Since then, ordered mesoporous metal oxides have been the topic of rapid discovery in materials chemistry, catalysis, chemical sensing, and separations.[3-6] Variations in the range of organic supermolecular templates and inorganic ions has led to many types of advanced materials.[7-9] Here, we report mesopore templating using mixtures of surfactants illustrated in Figure 1: nonionic n-octyl- β -D-glucopyranoside (C_8G_1) and cationic cetyltrimethylammonium bromide (CTAB). Sugar-based surfactants have many useful properties, but have not been extensively investigated as pore templates. In general, sugar-based surfactants are very hydrophilic because they contain a large number of hydroxyl groups in their headgroup. Sugars are also capable of multiple interactions with silica and transition metals that can lead to templating.[10] They are nontoxic and biodegradable, and can be synthesized from renewable resources.[11,12] They show considerable variety in micelle structure and phase behavior based on the anomeric and chiral form of the surfactant, in addition to the alkyl tail length and the type of carbohydrate head group.[11] In addition, carbohydrate surfactants are models for the types of nonionic molecules that may be useful for molecular imprinting, which transfers specific structural features from nonionic imprinting molecules into the inorganic framework.[13-15]

C_8G_1 is a commercially available surfactant and its phase behavior in water has been well characterized.[16,17] Štangar et al. reported the first and only attempt to use C_8G_1 as a pore template in mesoporous silica films prepared via dip-coating.[18] However, they found that C_8G_1 favors lamellar products, which is consistent with the large packing parameter of this

surfactant. The binary phase diagram of C_8G_1 in water[16,17] has only two narrow 2D hexagonal columnar phase (HCP) phase regions, from 28 to 32 wt% and from 59.5 to 70 wt%. The 2D HCP phase has a melting point of only 23°C,[19] which suggests that 2D HCP mesoporous silica cannot be prepared at or above room temperature with C_8G_1 alone. To overcome this problem, a mixture of surfactants may be capable of promoting hexagonal ordering. Cortes et al.[20] found that adding 1 wt% C_8G_1 to CTAB significantly expands the 2D HCP phase region in glycerol/water mixtures at $30.0\pm 0.1^\circ\text{C}$. The discovery of an extended 2D HCP region motivated us to further study the CTAB/ C_8G_1 /water ternary phase diagram. Preliminary studies (to be reported separately) show that this system has a large 2D HCP region, which is being explored as a guide to the rational synthesis of mesoporous silica materials with mixed CTAB/ C_8G_1 surfactants as templates.

In this work, we will first show that mixed CTAB/ C_8G_1 surfactants can indeed be used as templates to make 2D HCP structured porous metal oxides via nanocasting. Surfactant-templated oxides were first prepared by sol-gel reaction-induced precipitation of silica precursors from dilute (<30 wt.%) surfactant solutions,[21-23] by a mechanism best described as co-assembly.[24,25] However, we use a method similar to the microemulsion-gel method[26] called “nanocasting” in which sol-gel polymerization occurs directly in a lyotropic liquid crystal phase.[27] In this process, a concentrated surfactant solution is prepared, and an alkoxide precursor is added which hydrolyzes and slowly condenses to generate the oxide. The alcohol produced by hydrolysis usually destroys the lyotropic order, but by evaporating the alcohol, it is possible to recover a material that mimics the structure of the original liquid crystal[28-30] so that the size, connectivity and ordering of the final nanoscopic pore system can be predicted *a priori* based on the aqueous surfactant phase

diagram. The high surfactant concentration used for nanocasting helps to drive co-assembly in the presence of weak surfactant-silica interactions present in nonionic surfactant systems.[32-35] Because the liquid structure is lost during hydrolysis and regained during drying, the method resembles the evaporation-induced self-assembly process.[31] Recently, nanocasting has been extended by using mixed immiscible template to generate hierarchical pore systems,[36,37] and mixed short-chain alcohols and block copolymers to control the pore size.[38] Here, we will for the first time perform nanocasting with a mixture of sugar-based and cationic surfactants.

In this study, calcination is used to remove the surfactants from all samples (for consistent comparison). However, if mixed surfactants are to be used to impart functionality to the porous oxide, it will be necessary to remove the surfactant by extraction rather than by calcination. Because an acid medium is used for nanocasting, the as-made materials require an extremely long time to condense sufficiently to allow extraction.[39] We hypothesized that exposing the samples to ammonia vapor at 50 °C would be a mild post-synthesis treatment that would stabilize the silica network to allow extraction. Ammonia/water vapor treatment of silica films without surfactant templates has been shown to improve their degree of crosslinking and mechanical strength.[40] Ammonia hydrothermal treatment has been used before to stabilize the structure of acid-catalyzed surfactant-templated samples[41,42] but here we use vapor treatment to limit the extent of pore distortion caused by dissolution of silica and Ostwald ripening.[41] A known side-effect of ammonia treatment with cationic surfactants is pore expansion[41,42] and this effect has been exploited to manipulate the pore size of surfactant-templated silica using various amines added before and after synthesis.[43] Attempting to use a new, mild ammonia vapor treatment leads to much greater pore

expansion when C_8G_1 is added than for pure CTAB. The magnitude of the expansion with C_8G_1 can be enough to introduce pore defects, but we will demonstrate strategies to limit its extent. Because pore expansion may or may not be desirable (depending on the application), we will explore the mechanism of expansion using different mixtures of ionic and nonionic surfactants to manipulate the charge density at the silica/surfactant interface. We will show that the Maillard reaction between ammonia and the sugar headgroups plays a surprisingly important role, even under mild treatment conditions.

Experimental

Materials

Cetyltrimethylammonium bromide, CTAB (99.0%, Sigma), tetramethyl orthosilicate, TMOS (>99.0%, Sigma), n-octyl- β -D-glucopyranoside, C_8G_1 (\geq 99.0%, Fluka), concentrated aqueous ammonia (28 wt%, Fisher Scientific), deionized ultrafiltered (DIUF) water (Fisher Scientific), and normalized 0.01 N hydrochloric acid solution (Alfa) were used as received.

Synthesis Procedure

The nanocasting procedure was similar to that reported in the literature.[27] In all samples, the ratio of total surfactant to water was 50 wt%. Typically, 1 g CTAB and X g C_8G_1 were dissolved in (1+X) g of aqueous hydrochloric acid (pH=2) with stirring, and the mixture was heated at 50 °C for at least 30 min to reach a liquid crystal-like state. Then TMOS was added to these mixtures. The amount of TMOS used was always less than 0.25 mole equivalents with respect to the water. In this way, the water content in the mixture was slightly higher than that required for the complete hydrolysis of the TMOS. Hydrolysis with stirring proceeded for 20 min, and then the transparent mixture was exposed to a gentle vacuum to remove the methanol. The resulting viscous solution was transferred into a Petri dish to form

a film and aged at 50°C in a temperature-controlled digital dry bath for 48 hr. The surfactant templates were removed by calcination in air at 550°C for 6 hr.

Post-synthesis treatment of some as-made samples was accomplished by first spreading the as-made sample on a watch glass, which was then placed into a Petri dish. A measured amount of concentrated aqueous ammonia (28 wt%) was added below the watch glass without touching the sample, and the dish was covered with parafilm and stored at 50 °C overnight. While the long-term goal of doing this is to allow surfactant extraction, we still calcined the ammonia-treated samples, for direct comparison with samples that were not treated with ammonia. The quantities of all materials used are reported in Table 1.

Characterization Methods

The long-range order of the samples was characterized with a Siemens 5000 x-ray diffractometer using 0.154098 nm Cu-K α radiation, a graphite monochromator, and a scan rate of 1 °/min. Nitrogen adsorption-desorption isotherms were obtained at -196 °C using a Micromeritics Tristar 3000 automated adsorption instrument. The samples were degassed at 120 °C for 4 hr prior to analysis. For transmission electron microscopy (TEM), samples were ground and loaded onto lacey carbon grids for analysis using a JEOL 2010F instrument at a voltage of 200 kV. Fourier transform infrared (FTIR) spectra were obtained with a desiccated and nitrogen-purged ThermoNicolet Nexus 470 infrared spectrometer with a DTGS detector. Samples were finely ground and diluted to 1 wt% with KBr powder before being pressed into translucent pellets with a hand press. UV-visible (UV-vis) spectroscopy was performed with a HP8453 UV-vis spectrophotometer using disposable UV-transparent plastic cuvettes from Fisher Scientific. For UV-vis analysis, the organic reaction products and surfactants were extracted with dry ethanol, and the extracts were diluted 2-fold before testing. The phase

behavior of ternary CTAB/C₈G₁/water mixtures was investigated using a Zeiss Axioskop microscope with crossed polarizing filters, and the images were recorded using a Nikon Coolpix 995 digital camera. Microscope samples were prepared by weighing the required amounts of surfactants and water into PVC vials which were sealed and homogenized in an ultrasonic bath before being transferred into silicone spacers and sandwiched between a glass slide and cover slip. To ensure that no evaporation occurred, each side of the coverslip was sealed with vacuum grease. The samples were aged in a temperature-controlled dry bath for 24 hr to reach equilibrium before analysis. The temperature of the sample in the microscope was maintained with a heated stage during analysis.

Results and Discussion

Before attempting to make materials via the nanocasting procedure, we first analyzed the phase behavior of a number of ternary CTAB/C₈G₁/water samples using polarized optical microscopy (POM). As an example, Figure 2 shows the POM image of a mixture consisting of 50 wt% , water, 40 wt% CTAB, and 10 wt% C₈G₁ at 50 °C after equilibration for 24 hr. Figure 2 shows a fanlike texture, which is a typical 2D HCP pattern. The phase behavior study using POM suggests that it may be feasible to prepare materials with 2D HCP structure using the CTAB/C₈G₁ compositions investigated here (summarized in Table 1).

Nanocasting using CTAB/C₈G₁ without NH₃ vapor post-treatment

The nitrogen adsorption isotherms for a series of calcined samples with varying C₈G₁ content are shown in Figure 3. In this series, the C₈G₁ content increases from MST-1C through MST-6C. All samples have typical reversible type IV isotherms.[44] A sharp inflection between relative pressure $p/p_0 = 0.1$ and 0.2 corresponds to capillary condensation in uniform mesopores. The sharpness of this step reflects the uniformity of the mesopores. The

inflection point occurs around 0.135 for all samples except MST-6C, whose isotherm shows an inflection at $p/p_0 = 0.116$. The pore size distributions of all samples were calculated from adsorption data using the BJH method with a modified Kelvin equation and the Harkins-Jura equation for film thickness (also known here as KJS pore size distributions).[45,46] The pore size distributions of samples MST-1C through MST-5C are centered around 2.68 nm with a full-width at half-maximum (FWHM) of 1.2 nm. Sample MST-6C also has a narrow pore size distribution, but a smaller pore size of 2.58 nm.

The XRD patterns for this series of calcined samples are shown in Figure 4. All of the samples synthesized with different concentrations of C_8G_1 show one intense (100) reflection and weaker (110) and (200) reflections, indicating that the prepared materials contain well-ordered 2D HCP pores. However, with increasing C_8G_1 content, the peak intensity decreases and the higher order reflections become less resolved, showing that the mesopore ordering decreases. This is consistent with C_8G_1 having a higher packing parameter than CTAB, which causes it to favor the lamellar phase at this temperature.[16] TEM micrographs (Figure 5 shows examples for MST1C and MST3C) confirm that the mixed-surfactant-templated silica materials contain well-ordered, 2D HCP pores.

To learn more about the pore structure, we calculate other structure parameters based on the nitrogen adsorption measurements of the calcined materials. Using the methods of Sayari et al.,[47] we obtain the mesopore diameter w_d , primary mesopore volume V_p , total surface area S_t , and external surface area S_{ex} by making and analyzing α_s plots. The standard reduced nitrogen adsorption isotherm data (α_s) for the reference material, LiChrospher Si-1000 silica, are taken from Jaroniec et al.[48] All of the results, with the d_{100} spacings obtained from XRD, are listed in Table 2. Some interesting trends emerge in this set of data. The w_d values

vary little, and agree with the estimates of pore diameter calculated from the KJS pore size distributions (W_{KJS}), which is consistent with the pores being cylindrical.[46] All of the d_{100} values are smaller than those of MCM-41 synthesized by reaction-induced precipitation under basic conditions.[47] The values decrease from 3.04 to 2.74 nm as the C_8G_1 content increases. The wall thickness decreases monotonically from 0.84 to 0.58 nm as the C_8G_1 content increases. Also, the primary pore volume increases from 0.56 to 0.66 cm^3/g between samples MST-1C and MST-5C. According to Polarz et al.,[49] nanocasting should result in a 1:1 imprint of the organic template. Therefore, we interpret the changes in pore texture between sample MST-1C and MST-5C as being caused by an increase in the number of micelles in the synthesis solution as C_8G_1 is added. The size of the micelles (which determines the pore size) remains constant with even up to 0.3 g C_8G_1 per gram of CTAB. This suggests that C_8G_1 is readily substituted for CTAB in the micelles even though the total amount of surfactant increases. Increasing micelle number density explains both the increase in specific pore volume and the decrease in wall thickness as C_8G_1 is added.

Nanocasting using CTAB/ C_8G_1 with NH_3 vapor post-treatment

In this section, we compare samples prepared under the same experimental conditions as samples MST-1C through MST-6C, but with the NH_3 vapor post-treatment described in the Experimental section. Figure 6 shows the nitrogen adsorption isotherms and pore size distributions for this series (MST-1NC through MST-6NC). Ammonia treatment causes significant changes in both isotherms and pore size distribution. All isotherms are still of type IV, but type H2 triangular hysteresis loops with steep desorption branches begins to appear when the amount of C_8G_1 used exceeds 10% of the amount of CTAB (e.g. sample MST-3NC). The area enclosed by the hysteresis loop increases as the C_8G_1 concentration

increases. The H2 hysteresis loop is associated with a nonuniform pore diameter, or with branching between pores. Therefore, as more C₈G₁ is used during the synthesis, we find evidence that ammonia treatment causes more distortion of the pores. The pore size distributions also show that the pore diameter and the breadth of the pore size distribution increase with more C₈G₁ in the synthesis solution. The peak pore size (W_{KJS}) increases monotonically, from 3.06 to 4.18 nm, as the C₈G₁ content increases (see Table 2). These pore sizes are greater than those found in the samples that were not treated with ammonia, but apparently more C₈G₁ allows more distortion to be caused by ammonia treatment.

The XRD patterns for this series of samples are shown in Figure 7. The long-range order is improved after NH₃ vapor treatment, even for those samples with higher C₈G₁ contents. The pore texture parameters and d_{100} spacings for this series of samples are given in Table 2. As the C₈G₁ content of the materials increases, both the pore size (W_{KJS}) and the primary mesoporous volume (V_p) increase. The pore diameters calculated based on the surface area and pore volume (w_d) and W_{KJS} begin to disagree when the amount of C₈G₁ exceeds 10% of the CTAB amount, which indicates that the pore structure gradually departs from perfect 2D HCP cylinders. The loss of perfect pore uniformity is correlated with the gradual increase in the size of the H2 hysteresis loop in the adsorption isotherms. There are a few possible reasons for the H2 hysteresis loops.[44] One possibility is the partial collapse of pores during ammonia vapor treatment, which would shrink some of the pores into the micropore range. However, we can rule this out because of the absence of any detectable micropore filling at low p/p_0 . Another possible reason for the H₂ hysteresis loop is increased pore connectivity.[46] We doubt this interpretation because even the sample with the highest amount of C₈G₁ in this series (MST-6NC) still shows a strong d_{100} peak in the XRD patterns,

and long cylindrical pores in the TEM image (Figure 5). Therefore, we interpret the H_2 hysteresis loops as coming from variations in pore diameter along the length of the pores. This is a variation of the ink bottle pore shape interpretation, and is consistent with the TEM images (for example, MST-6NC in Figure 5).[44,50] This interpretation is consistent with more extensive expansion of the micelles during ammonia treatment of the samples with more C_8G_1 . This expansion creates larger, non-uniform pores.

To learn more about the chemical changes induced by ammonia treatment, we analyzed samples by FTIR. This was in part motivated by the observation that samples containing more than 0.1 g C_8G_1 : 1 g CTAB developed a brown color during NH_3 treatment (discussed more below) which was lost upon calcination. Figure 8 shows the infrared spectra for one representative sample (with a surfactant mixture containing 0.2 g C_8G_1 : 1 g CTAB). Bands at 2919 cm^{-1} and 2850 cm^{-1} are attributed to CH_2 asymmetric and symmetrical stretching, respectively, of the mixed surfactants.[51] Bands around 1486 cm^{-1} are attributed to surfactant deformation modes.[52] After calcination, these peaks disappear, showing that surfactants are removed completely. The band at 963 cm^{-1} has previously been attributed to the asymmetric CH_3-N^+ stretch of the surfactant.[53] The band at 951 cm^{-1} is attributed to Si-OH stretching,[54] and the 963 cm^{-1} band may also be associated with Si-OH. In addition, all three samples exhibit a broad, asymmetric Si-O-Si stretching band at $1020\text{-}1090\text{ cm}^{-1}$.[53] The sharp Si-O-Si stretching peak maximum is shifted and intensified to higher wavenumber, from 1067 to 1069 cm^{-1} , which suggests enhanced sol-gel condensation after ammonia treatment. The appearance of a new siloxane LO_3 stretching band[54] at 1233 cm^{-1} after ammonia treatment shows that the condensation of remaining silanol groups in the silicate phase becomes more complete.[53] Also with ammonia treatment, the broad OH stretching

band near $\sim 3300\text{ cm}^{-1}$ shifts to $\sim 3500\text{ cm}^{-1}$, suggesting weaker hydrogen bonding among the hydroxyls.[54,55] This is consistent with increased condensation among the silanols due to ammonia exposure. Aside from the increase in condensation of the siloxane network, no other chemical change can be clearly deduced from the FTIR spectra of the ammonia-treated samples.

Based on the analysis of the ammonia-treated samples in Figs. 5-8, we determine that ammonia strengthens the silica network by increasing the degree of siloxane condensation, but that with larger amounts of the glucoside surfactant, more pore expansion and greater disorder is introduced. The development of pore shape distortion is correlated with the presence of hysteresis loops. We hypothesize that pore expansion is enhanced by the reaction of NH_3 with C_8G_1 in materials with soft, thin walls. To test this hypothesis, we next examine the effects of the amounts of NH_3 and TMOS on the expansion of the pores.

Effect of the amount of ammonia vapor

One representative mixed surfactant composition (0.2 g C_8G_1 : 1 g CTAB) was chosen to investigate of the effect of NH_3 vapor amount used. Three new samples (MST-7NC through MST-9NC) were synthesized for this purpose. Figure 9 shows the nitrogen sorption isotherms and pore size distributions for a series of samples treated using different amount of NH_3 vapor (for specific experimental conditions see Table 1). Adsorption isotherms clearly show that the occurrence and development of a H2 hysteresis loop are closely related with the amount of NH_3 used during post synthesis. With the smallest amount of ammonia employed in this series (MST-7NC), no hysteresis loop is found. However, with more ammonia used to treat the as-made materials, the hysteresis loops grow until, at a certain size, the amount of ammonia shows little influence on the size of the hysteresis loop.

Paralleling the hysteresis loop development, the pore size distribution shifts towards larger pores and a broader distribution.

These results suggest that both the expansion of the pore size and the gradual condensation of silanol groups proceed at the same time during ammonia post-treatment. Because condensation is slow under acidic conditions, the as-made silica materials have flexible walls which would easily collapse during surfactant extraction. During the post-synthesis treatment described here, NH_3 can interact with the micelles present in the surfactant-rich nanochannels to expand the pores (see below for more discussion of the mechanism). At the same time, ammonia and water adsorb at the silica/surfactant surface, thus increasing the effective pH value and enhancing the condensation rate to solidify the network. The competition between expansion and rigidification induced by ammonia leads to increased expansion until a plateau pore size is reached which is controlled by the silica condensation rate (3.69 nm for the series of sample under study). The XRD patterns for this series of samples (not shown) all show HCP ordering, so the amount of ammonia has little effect on the long-range order of the materials. Table 2 shows the other pore texture parameters and the XRD-derived d_{100} spacing.

Effect of the amount of silica precursor

The precursor amount in the system is critical to the formation of an ordered material, especially at a high concentration of surfactants.[56] In the nanocasting procedure, the template assembles with silicates in a concentrated phase in a way that mimics the formation of aqueous liquid crystals. Changing the amount of precursor should be analogous to changing the volume of water used in a liquid crystal. Thus, nanocasting provides a

controllable way to study the effect of precursor content on the wall thickness and its effect on the stability of the resulting material.

One representative mixed surfactant composition (0.1 g C_8G_1 : 1 g CTAB) was chosen for the investigation of the effect of precursor content during ammonia treatment. Three new samples were prepared in this series, MST-10NC through MST-12NC. Figure 10 shows the nitrogen adsorption and desorption isotherms and pore size distributions for this series after ammonia treatment and calcination. A smaller amount of precursor leads to a larger hysteresis loop in the samples. The isotherm of the sample prepared with the least amount of precursor (MST-10NC) has a hysteresis loop spanning a large range of relative pressure, which indicates extensive swelling and deformation of the pores caused by pore expansion during ammonia treatment. With the largest amount of precursor (MST-12NC), no indication of a hysteresis loop is found after ammonia treatment. All these results show that the strength of the pore walls can be adjusted by precursor content if correct proportions of precursor, surfactant and water are used. Presumably, less distortion can be associated with thicker (stronger) pore walls. Like the other samples prepared with ammonia treatment, the presence of a hysteresis loop is associated with larger pores and a broader pore size distribution. The X-ray diffraction patterns for this series of samples are shown in Figure 11. The sample with the least precursor (MST-10NC) loses its long-range order after ammonia treatment, which is consistent with its adsorption isotherm. For the other two samples, some long-range order is preserved, but not a perfect 2D HCP pattern because the pore shape has been distorted by ammonia treatment. Other structural parameters are listed in Table 2.

Mechanism of pore expansion with glucopyranoside surfactant

It has previously been demonstrated that hydrothermal (>100 °C) post-synthesis treatment with ammonia can improve the order and stability of mesoporous materials made with cationic surfactants under acidic conditions.[41] This can be explained by the replacement of weak S^+XI^+ electrostatic interactions and hydrogen bonding with stronger S^+I interactions at the silica-surfactant interface (where S represents a surfactant, I represents an inorganic species, and X represents a counterion).[41,57] At the same time, hydrothermal ammonia treatment leads to expansion of the pores in the materials for reasons that are not fully understood. The main explanation cited in the literature is increased hydration of silica.[58] Swelling of the micelle cores by ammonia (uncharged NH_3) may play a role similar to the intentional amine swelling reported by Sayari et al.[43] Decomposition of the pore template has also been cited as a cause for extensive swelling for cetylpyridinium chloride templating.[42] However, none of these effects explains why we see a difference in expansion depending on the quantity of C_8G_1 used.

In the present case, we are for the first time exploring the vapor-phase ammonia treatment at a mild temperature of 50 °C of an acid-catalyzed material prepared with a mixed surfactant template. As described above, when CTAB is used as the sole template, post-synthesis ammonia vapor treatment can improve the hexagonal order of the meso-structure and slightly increase the pore diameter (around 0.4 nm). There is no indication of the development of a hysteresis loop in the ammonia-treated CTAB sample. However, when sugar-based surfactant C_8G_1 is introduced to the template system, a large increase of pore diameter (up to 1.6 nm), broadening of the pore size distribution, development of a hysteresis loop, and (sometimes) loss of long-range order are observed. The degree of these variations depends

strongly on the amounts of C_8G_1 , ammonia, and precursor employed. To elucidate the mechanism causing the change of porosity during ammonia vapor treatment, we conducted experiments to test two hypotheses: (1) that because C_8G_1 is non-ionic, the degree of stabilization of the silica-surfactant interface is reduced, allowing the micelles to swell more as CTAB is replaced in the system; and (2) that a reaction analogous to the Maillard reaction occurs, as suggested by the brown color formation after ammonia vapor treatment of the surfactant/silicate composites prepared with more than 0.1 g C_8G_1 per g CTAB.

To test the first hypothesis, we investigated the influence of ammonia vapor treatment on a series of as-made 2D HCP structured materials made with various surfactants, as shown in Table 3. Those samples were prepared by nanocasting under the same experimental conditions as the CTAB/ C_8G_1 samples in Table 1. From the Table 3, at least three conclusions can be reasonably drawn. First, if a single template was used, whether cationic (CTAB) or non-ionic (Brij56), the pore size expansion is almost the same, only around 0.4 nm. However, when a cationic surfactant (CTAB) and a non-ionic surfactant (Brij56, Brij52, or C_8G_1) are mixed together as templates, the pore size expands more as the amount of nonionic surfactant increases, which indicates that our first hypothesis is correct. Second, when combined with a non-ionic surfactant (C_8G_1) as template, a cationic surfactant (C_n TAB series, $n = 10, 12, 16$) with a longer tail permits a greater degree of pore expansion. In addition, the type of headgroup on the cationic surfactant influences the degree of pore expansion; a trimethylammonium headgroup (as in C_{16} TAB) permits greater expansion than a pyridinium headgroup (as in HPBr). All of these results indicate that the change of physical interactions occurring both inside the core of the micelles and at interfaces between micelles and silicate during ammonia vapor treatment influence the degree of pore

expansion. Our experiments do not allow us to directly determine whether NH_3 vapor causes pore expansion by swelling of the cores of the micelles or by expansion near the headgroups. Pure NH_3 is sparingly soluble in n-hexadecane (3 wt% at 30 °C),[59] so although ammonia is hydrophilic, either expansion mechanism is possible. Third, when C_8G_1 is combined with a cationic surfactant (C_nTAB or HPBr), significantly greater pore size expansion is observed than for other cationic-nonionic surfactant mixtures (~1.6 nm), accompanied with a color change from white to brown and the appearance of a hysteresis loop in the adsorption isotherm. As discussed above, the degree of pore expansion and the size of the hysteresis loop increase with increasing C_8G_1 content. Obviously, all of these changes can not be simply explained by the first hypothesis.

To test the second hypothesis that a Maillard-like reaction occurs during ammonia vapor treatment of C_8G_1 -containing samples, we analyzed the UV-vis and FTIR spectra of products extracted with ethanol from the as-synthesized samples. Figure 12 show the UV-vis absorbance spectra of compounds extracted from materials prepared with 0.2 g C_8G_1 : 1 g CTAB (MST-5NC) before and after ammonia treatment. A significant increase in absorbance in the wavelength range 300-400 nm develops due to chemical reactions induced by treatment with ammonia vapor. The peak occurs in the range associated with aromatic compounds produced by reactions between carbohydrates and amines known collectively as the Maillard reactions.[60] IR spectroscopy also shows evidence of new bands in the “fingerprint” region of the spectrum of the material extracted from the ammonia-treated sample, suggesting that some reaction happened during ammonia vapor treatment. Unfortunately, the infrared bands could not be clearly assigned to one reaction product, but may be associated with a variety of organic groups.

The Maillard reaction was first described as a reaction between reducing sugars and amino acids,[61] but now has been extended to include many other carbohydrate and amine groups. The mechanism of the reaction is quite complex, and involves a series of reactions that yield a multicomponent mixture of organic compounds. The precise mechanism and distribution of reaction products remains an open topic of research in carbohydrate chemistry. However, it is well documented that volatile heterocyclic compounds usually form during the reaction, such as pyrazines, pyrroles, pyridines, oxazoles and oxalines.[62] Some of these uncharged, low molecular weight organic species would be expected to expand the micelles, leading to the extensive changes in pore structure that we have observed. This mechanism is similar to the mechanism of pore expansion proposed by Yuan et al. for expansion of cetylpyridinium chloride-templated materials.[42,47,63] Since the glucopyranoside heagroups of C_8G_1 should be able to react with ammonia to form many types of volatile compounds such as pyrazines, imidazole, furfuryl alcohol etc.,[64] we propose that the Maillard reaction between the sugar-based surfactant C_8G_1 and ammonia vapor at the silica surface causes enhanced pore expansion and the development of hysteresis loops in the nitrogen adsorption isotherms of the samples. This is consistent with all observations in this paper, including an increase in expansion with more C_8G_1 , an increase in expansion with more ammonia, and a decrease in pore expansion when a greater amount of precursor is used to make stronger pore walls. Surprisingly, the reaction seems to be facilitated by intimate contact between silica and C_8G_1 . Pure C_8G_1 or physical mixtures of MCM-41 with C_8G_1 and CTAB do not develop a brown color upon ammonia vapor treatment at 50 °C. Enhanced adsorption of ammonia at the silanol surface or chemical bonding between silica and the sugar[65] may help to explain the enhancement of the Maillard reaction in silica containing a carbohydrate template.

Conclusions

A series of siliceous materials with 2D hexagonal columnar mesopores were synthesized using mixed cationic CTAB and nonionic sugar-based surfactant C₈G₁ as templates via the nanocasting method. The effects of ammonia vapor treatment of the as-made samples at a mild temperature (50 °C) was observed. Ammonia vapor treatment led to retention or improvement of the long-range order among the pores as assessed by x-ray diffraction. It was found not only that the pore diameters were enlarged after ammonia treatment, but that the degree of pore size expansion could be controlled by adjusting the amount of C₈G₁ in the mixed surfactant system. A larger amount of C₈G₁ led to greater pore expansion, but too much expansion led to a loss of pore uniformity. The degree of expansion of the pores could be reduced by using less ammonia vapor or a larger amount of silica precursor. Based on a series of investigations with other nonionic surfactants (Brij56 and Brij52), we conclude that pore expansion is associated not only with a change in the physical interactions between silica and the surfactants, but also with the occurrence of the Maillard reaction between the sugar-based surfactant C₈G₁ and ammonia vapor at the surface of silica. Nonpolar, low-molecular weight byproducts of this reaction would be expected to swell the micelles, leading to the observed expansion of pore size, and in extreme cases, degradation of pore uniformity. Controlled use of the pore expansion of carbohydrate / cationic surfactant mixtures may be useful for tuning mesoporous metal oxides for size exclusion applications. However, if the goal is to preserve the structure templated by carbohydrate-based surfactants, one must be cautious to avoid the Maillard reaction even under mild conditions. It is possible that silica catalyzes this sugar transformation reaction.

Acknowledgment

We gratefully acknowledge financial support from the National Science Foundation (NSF) (Grant Nos. DMR-0210517 and EAR-0521405) and we thank Dr. Bing Tan for help with TEM imaging. We thank Prof. K.W. Anderson for providing access to the optical microscope and Prof. B.L. Knutson for access to the UV-vis spectrophotometer.

References

- (1) J.S. Beck, J. C. Vartuli, W. J. Roth, M. E. Leonowicz, C. T. Kresge, K. T. Schmitt, C.T-W. Chu, D. H. Olson, E.W. Sheppard, S.B. McCullen, J.B. Higgins, J.L. Schlenker, *J. Am. Chem. Soc.* 114 (1992) 10834.
- (2) C.T. Kresge, M.E. Leonowicz, W.J. Roth, J.C. Vartuli, J. S. Beck, *Nature* 359 (1992) 710.
- (3) A. Corma, D. Kumar, in *Mesoporous Molecules Sieves 1998*, L. Bonneviot, F. Béland, C. Danumah, S. Giasson, and S. Kaliaguine (eds.), *Studies Surface Sci. Catal.* 117 (1998) 201.
- (4) X.S. Zhao, G.Q. Lu, G.J. Millar, *Ind. Eng. Chem. Res.* 35 (1996) 2075.
- (5) C.G. Guizzard, A.C. Julbe, A. Ayrat, *J. Mater. Chem.*, 9 (1999) 55.
- (6) U. Ciesla, F. Schüth, *Micropor. Mesopor. Mater.* 27 (1999) 131.
- (7) S. Inagaki, S. Guan, T. Ohsuna, O. Terasaki, *Nature* 416, (2002) 304.
- (8) Q. Huo, D.I. Margolese, U. Ciesla, D.G. Demuth, P. Feng, T.E. Gier, P. Sieger, A. Firouzi, B.F. Chmekla, F. Schüth, G.D. Stucky, *Chem. Mater.* 6 (1994) 1176.
- (9) Y. Zhou, M. Antonietti, *Adv. Mater.* 15 (2003) 1452.
- (10) Y. Wei, J. Xu, H. Dong, J.H. Dong, K. Qiu, S.A. Jansen-Varnum, *Chem. Mater.* 11 (1999) 2023.
- (11) C. Stubenrauch, *Current Opinion Colloid Interface Sci.* 6 (2001) 160.
- (12) B. Hoffmann, G. Platz, *Current Opinion Colloid Interface Sci.* 6 (2001) 171.

- (13) C. Pinel, P. Loisel, P. Gallezot, *Adv. Mater.* 9 (1997) 582.
- (14) J.H. Jung, M. Amaiike, S. Shinkai, *Chem. Commun.* (2000) 2343.
- (15) M.A. Markowitz, P.R. Kust, G. Deng, P.E. Schoen, J.S. Dordick, D.S. Clark, B.P. Gaber, *Langmuir* 16 (2000) 1759.
- (16) P. Sakya, J.M. Seddon, R.H. Templer, *J. Phys. II France* 4 (1994) 1311.
- (17) F. Nilsson, O. Söderman, *Langmuir* 12 (1996) 902.
- (18) U.L. Štangar, M. Puchberger, N. Hüsing, *Mat. Res. Soc. Symp. Proc.* 726 (2002) 111.
- (19) G. Persson, H. Edlund, H. Amenitsch, P. Laggner, G. Lindblom, *Langmuir* 19 (2003) 5813.
- (20) A.B. Cortés, M. Valiente, *Colloid Polym. Sci.* 281 (2003) 319.
- (21) J.C. Vartuli, K.D. Schmitt, C.T. Kresge, W.J. Roth, M.E. Leonowicz, S.B. McCullen, S.D. Hellring, J.S. Beck, J.L. Schlenker, D.H. Olson, E.W. Sheppard, *Chem. Mater.* 6 (1994) 2317.
- (22) P.T. Tanev, T.J. Pinnavaia, *Science* 10 (1995) 865.
- (23) D. Zhao, Q. Huo, J. Feng, B.F. Chmelka, G.D. Stucky, *J. Am. Chem. Soc.* 120 (1998) 6024.
- (24) A. Firouzi, D. Kumar, L.M. Bull, T. Besier, P. Sieger, Q. Huo, S.A. Walker, J.A. Zasadzinski, C. Glinka, J. Nicol, D. Margolese, G.D. Stucky, B.F. Chmelka, *Science* 267 (1995) 1138.
- (25) A. Monnier, F. Schüth, Q. Huo, D. Kumar, D. Margolese, R.S. Maxwell, G.D. Stucky, M. Krishnamurty, P. Petroff, A. Firouzi, M. Janicke, B.F. Chmelka, *Science* 261 (1993) 1299.
- (26) S.E. Friberg, C.C. Yang, J. Sjöblom, *Langmuir* 8 (1992) 372.
- (27) G.S. Attard, J.C. Glyde, C.G. Göltner, *Nature* 378 (1995) 366.
- (28) C.G. Göltner, M. Antonietti, *Adv. Mater.* 9 (1997) 431.
- (29) C.G. Spickermann, *Top. Curr. Chem.* 226 (2003) 29.
- (30) Y. Zhou, M. Antonietti, *Chem. Mater.* 16 (2004) 544.

- (31) C.J. Brinker, Y.F. Lu, A. Sellinger, H.Y. Fan, *Adv. Mater.* 11 (1999) 579.
- (32) C.G. Göltner, B. Smarsly, B. Berton, M. Antonietti, *Chem. Mater.* 13 (2001) 1617.
- (33) H.P. Hentze, E. Krämer, B.;Berton, S. Förster, M. Antonietti, *Macromolecules* 32 (1999) 5803.
- (34) S.A. Bagshaw, E. Prouzet, T.J. Pinnavaia, *Science* 269 (1995) 1242.
- (35) S. Polarz, B. Smarsly, L. Bronsterin, M. Antonietti, *Angew. Chem. Int. Ed.* 40 (2001) 4417.
- (36) M. Antonietti, B. Berton, C. Göltner, H. Hentze, *Adv. Mater.* 10 (1998) 154.
- (37) M. Groenewolt, M. Antonietti, *Langmuir* 20 (2004) 7811.
- (38) P. Feng, X. Bu, D.J. Pine, *Langmuir* 16 (2000) 5304.
- (39) M.G. Song, J.Y. Kim, S.H. Cho, J.D. Kim, *Langmuir* 18 (2002) 6110.
- (40) G.M. Wu, J. Wang, J. Shen, Q.Y. Zhang, B. Zhou, Z.S. Deng, B. Fan, D.P. Zhou, F.S. Zhang, *J. Phys. D-Appl. Phys.* 34 (2001) 1301.
- (41) H.P. Lin, C.Y. Mou, S.B. Liu, C.Y. Tang, C.Y. Lin, *Micropor. Mesopor. Mater.* 44-45 (2001) 129.
- (42) Z.Y. Yuan, J.L. Blin, B.L. Su, *Chem. Comm.* (2002) 504.
- (43) A. Sayari, Y. Yang, M. Kruk, M. Jaroniec, *J. Phys. Chem. B* 103 (1999) 3651.
- (44) K.S.W. Sing, D.H. Everett, R.A.W. Haul, L. Moscou, R.A. Pierotti, J. Rouquérol, T. Siemieniewska, *Pure Appl. Chem.* 57 (1985) 603.
- (45) E.P. Barrett, L.G. Joyner, P. Halenda, *J. Am. Chem. Soc.* 73 (1951) 373.
- (46) M. Kruk, M. Jaroniec, *Langmuir* 13 (1997) 6267.
- (47) A. Sayari, P. Liu, M. Kruk, M. Jaroniec, *Chem. Mater.* 9 (1997) 2499.
- (48) M. Jaroniec, M. Kruk, *Langmuir* 15 (1999) 5410.
- (49) S. Polarz, Antonietti, M. *Chem. Comm.* (2002) 2593.

- (50) M. Kruk, M. Jaroniec, *Chem. Mater.* 13 (2001) 3169.
- (51) A.R. Hind, S.K. Bhargava, S.C. Grocott, *Langmuir* 13 (1997) 6255.
- (52) D.C. Calabro, E.W. Valyocsik, F.X. Ryan, *Micropor. Mater.* 7 (1996) 243.
- (53) D.R. Scheuing, J.G. Weers, *Colloids Surf.* 55 (1991) 41.
- (54) P. J. Innocenzi, *Non-Cryst. Solids* 316 (2003) 309.
- (55) T.M. Parrill, *J. Mater. Res.* 7 (1992) 2230.
- (56) N.R.B. Coleman, G.S. Attard, *Micropor. Mesopor. Mater.* 44-45 (2001) 73.
- (57) H.P. Lin, C.Y. Mou, S.B. Liu, *Adv. Mater.* 12 (2000) 103.
- (58) D. Khushalani, A. Kuperman, G. Ozin, K. Tanaka, J. Garces, M. Olken, N. Coombs, *Adv. Mater.* 7 (1995) 842.
- (59) K. Ishida, *Bull. Chem. Soc. Japan* 31 (1958) 143.
- (60) G. Grygierczyk, W. Fischer, M. Sajewicz, P. Kuś, R. Wrzalik, M. Czaja, M. Dziadek, T. J. Kowalska, *Planar Chrom.* 15 (2002) 449.
- (61) J.E. Hodge, *Ag. Food Chem.* 1 (1953) 928.
- (62) C.G.A. Davies, B.L. Wedzicha, C. Gillard, *Food Chem.* 60 (1997) 323.
- (63) Z.Y. Yuan, B.L. Su, *Colloids Surfaces A: Physicochem. Eng. Aspects* 241 (2004) 95.
- (64) C.K. Shu, B.M. Lawrence, in *Maillard Reactions in Chemistry, Food and Health*, B.M. Labuza, G.A. Reineccius, V. Monnier, J. O'Brien, J. Baynes (eds), Royal Society of Chemistry, Cambridge (1994) 140.
- (65) S.D. Kinrade, R.J. Hamilton, A.S. Schach, C.T.G. Knight, *J. Chem. Soc. Dalton Trans.* (2001) 961.
- (66) S. Brunauer, P.H. Emmett, E. J. Teller, *Am. Chem. Soc.* 60 (1938) 309.

Table 1 Experimental conditions for the synthesis of mixed-surfactant-templated (MST) silica materials. All samples were prepared with 1 g of CTAB and cured at 50 °C.

Sample name	Amount of C ₈ G ₁ (g)	Amount of H ₂ O (pH=2) (g)	Amount of TMOS (g)	Amount of ammonia (ml)
MST-1C	0	1	1.5	-
MST-2C	0.01	1.01	1.5	-
MST-3C	0.1	1.1	1.6	-
MST-4C	0.15	1.15	1.65	-
MST-5C	0.2	1.2	1.7	-
MST-6C	0.3	1.3	1.8	-
MST-1NC	0	1	1.5	1
MST-2NC	0.01	1.01	1.5	1
MST-3NC	0.1	1.1	1.6	1
MST-4NC	0.15	1.15	1.65	1
MST-5NC	0.2	1.2	1.7	1
MST-6NC	0.3	1.3	1.8	1
MST-7NC	0.2	1.2	1.7	0.5
MST-8NC	0.2	1.2	1.7	2
MST-9NC	0.2	1.2	1.7	2.5
MST-10NC	0.1	1.1	0.80	1.5
MST-11NC	0.1	1.1	1.6	1.5
MST-12NC	0.1	1.1	3.2	1.5

Table 2 Structural parameters of the mixed-surfactant-templated silica materials.^a

Sample Name	d ₁₀₀ (nm)	W _{KJS} (nm)	w _d ^b (nm)	V _p ^b (cm ³ /gm)	S _t ^b (m ² /gm)	S _{ex} ^b (m ² /gm)	S _{BET} (m ² /gm)	Wall thickness t (nm)
MST-1C	3.04	2.67	2.76	0.57	860	12.5	1390	0.84
MST-2C	2.96	2.67	2.66	0.56	827	12.9	1370	0.75
MST-3C	2.92	2.68	2.66	0.59	860	8.6	1130	0.70
MST-4C	2.90	2.68	2.64	0.59	867	10.8	1170	0.67
MST-5C	2.87	2.68	2.68	0.66	945	3.6	1220	0.63
MST-6C	2.74	2.58	2.47	0.56	866	5.4	1060	0.58
MST-1NC	3.29	3.06	3.14	0.74	864	10.9	1000	0.74
MST-2NC	3.22	3.18	3.08	0.75	809	11.0	914	0.54
MST-3NC	3.25	3.33	3.12	0.76	802	11.9	939	-
MST-4NC	3.34	3.54	3.29	0.87	823	18.1	930	-
MST-5NC	3.27	3.83	3.27	0.97	839	20.3	902	-
MST-6NC	3.34	4.18	3.34	0.96	706	16.7	723	-
MST-7NC	3.15	3.12	3.0	0.74	861	16.9	1060	0.52
MST-8NC	3.34	3.69	3.27	0.85	748	20.4	895	-
MST-9NC	3.37	3.69	3.31	0.87	769	18.6	838	-
MST-10NC	-	3.84	-	0.62	683	119.2	724	-
MST-11NC	3.34	3.7	3.26	0.83	768	18.0	832	-
MST-12NC	3.27	3.39	3.03	0.64	710	10.9	793	-

^a d₁₀₀ = (100) spacing determined by XRD, W_{KJS} = pore diameter at peak of KJS pore size distribution, w_d = pore diameter calculated from $w_d = 1.213d_{100}(\rho V_p/(1+\rho V_p))^{1/2}$, V_p = primary mesopore volume, S_t = total specific surface area, S_{ex} = external specific surface area, S_{BET} = BET surface area,[66] and $t = (2/\sqrt{3})d_{100}-W_{KJS}$.

^b Calculated using α_s comparative nitrogen adsorption plots.[47]

Table 3 Comparison of characteristics of mesoporous silica prepared with different surfactants.

Surfactant system (masses used)	Calcined samples				Ammonia vapor treated ^a + calcined samples				
	W _{KJS} (nm)	S _{BET} (m ² /g)	V _p (cm ³ /g)	Hysteresis loop?	W _{KJS} (nm)	S _{BET} (m ² /g)	V _p (cm ³ /g)	Hysteresis loop?	Color change during NH ₃ treatment
C ₁₆ TAB (1)	2.67	1387.1	0.57	no	3.06	1000.9	0.74	no	white →white
Brij56 (1)	3.26	660.7	0.52	no	3.67	647.0	0.60	no	white →white
C ₁₆ TAB/Brij56 ^b (1:0.1)	2.68	891.5	0.47	no	3.04	782.0	0.52	no	white →white
C ₁₆ TAB/Brij56 ^b (1:0.2)	2.68	869.3	0.45	no	3.41	802.5	0.62	no	white →white
C ₁₆ TAB/Brij56 ^b (1:0.3)	2.68	780.0	0.41	no	3.68	837.4	0.78	no	white →white
C ₁₆ TAB/Brij52 ^b (1:0.3)	2.83	770.4	0.48	no	3.53	654.6	0.64	no	white →white
C ₁₆ TAB/C ₈ G ₁ (1:0.3)	2.58	1059.9	0.56	no	4.18	723.4	0.96	yes	white →brown
C ₁₂ TAB/C ₈ G ₁ (1:0.3)	2.18	768.1	0.42	no	3.53	714.5	0.78	yes	white →brown
C ₁₀ TAB/C ₈ G ₁ ^c (1:0.3)	< 2.00	621.7	0.35	no	2.82	839.3	0.63	yes	white →brown
HPBr/C ₈ G ₁ ^d (1:0.3)	2.68	881.3	0.45	no	3.53	794.0	0.77	yes	white →brown

^a All samples here were treated with 1 ml of concentrated ammonia as described in the experimental section.

^b Brij52 and Brij56 = C₁₆H₃₃O(C₂H₄O)_nH where n ~ 2 and 10, respectively.

^c For only this sample, no 2D HCP order was detected by XRD before or after ammonia treatment. All other samples had 2D HCP order.

^d HPBr = Hexadecylpyridinium Bromide.

Figure Captions

Figure 1. Molecular structures of surfactants used for materials synthesis.

Figure 2. Polarization contrast optical micrograph of a mixture of 50 wt% water, 40 wt% CTAB and 10 wt% C₈G₁ at 50 °C (200x magnification).

Figure 3. Nitrogen adsorption isotherms of calcined MST-#C samples.

Figure 4. X-ray diffraction (XRD) patterns for calcined MST-#C samples.

Figure 5. Representative transmission electron micrographs of MST series samples after calcination. The inset is a Fourier transform of the indicated region.

Figure 6. (L) Nitrogen adsorption isotherms and (R) KJS pore size distributions of calcined MST-#NC samples after ammonia treatment.

Figure 7. XRD patterns for series MST-#NC samples after ammonia treatment and calcination.

Figure 8. FTIR spectra for one representative mixed surfactant composition (1 g CTAB : 0.2 g C₈G₁) (a) as-made material before ammonia treatment, (b) as-made material after ammonia treatment, and (c) mesoporous silica material after calcination.

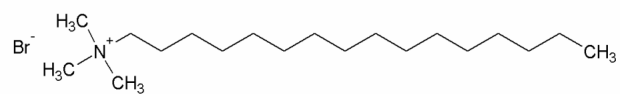
Figure 9. (L) Nitrogen adsorption isotherms and (R) KJS pore size distributions for samples treated with different amounts of ammonia (increasing from bottom to top) after calcination.

Figure 10. (L) Nitrogen adsorption isotherms and (R) KJS pore size distributions for samples synthesized with different amount of precursor (increasing from bottom to top).

Figure 11. XRD patterns for samples synthesized with different amounts of precursor (increasing from bottom to top).

Figure 12. The UV-visible absorbance spectra of ethanol solutions extracted from uncalcined materials prepared with 0.2 g C₈G₁ : 1 g CTAB and with or without ammonia treatment.

Cetyltrimethylammonium Bromide (CTAB)



Octyl-β-D-Glucoopyranoside (C₈G₁)

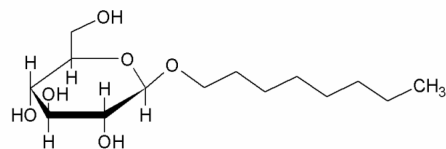


Figure 1 Molecular structures of surfactants used for materials synthesis.

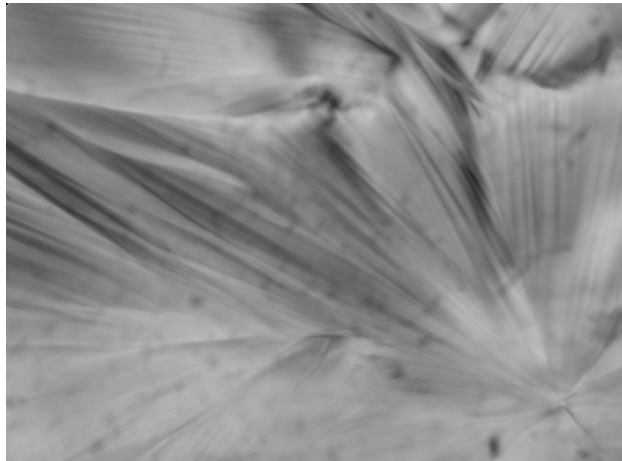


Figure 2. Polarization contrast optical micrograph of a mixture of 50 wt% water, 40 wt% CTAB and 10 wt% C₈G₁ at 50 °C (200x magnification).

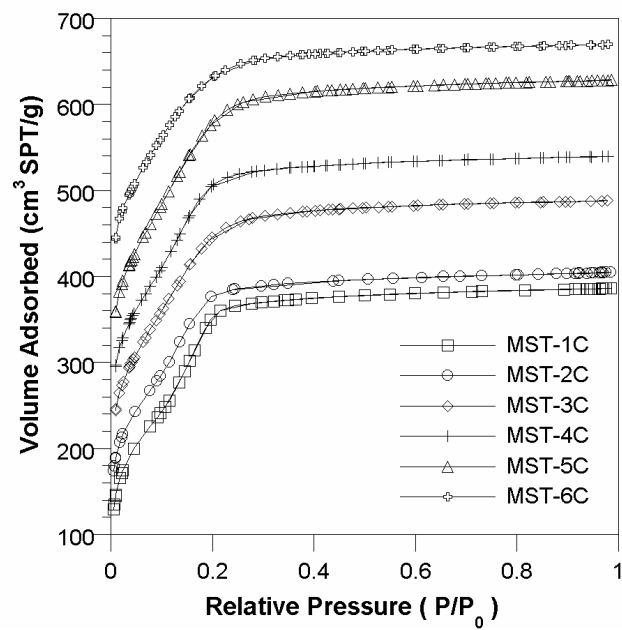


Figure 3. Nitrogen adsorption isotherms of calcined MST-#C samples.

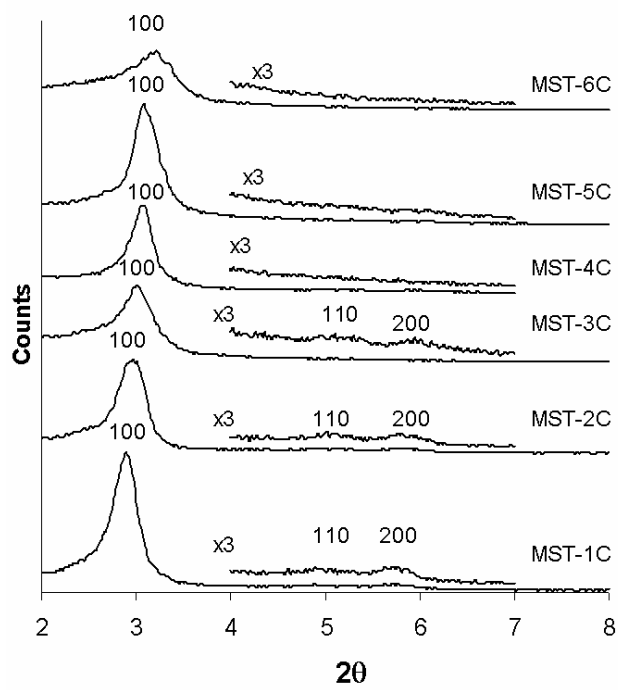


Figure 4. X-ray diffraction (XRD) patterns for calcined MST-#C samples.

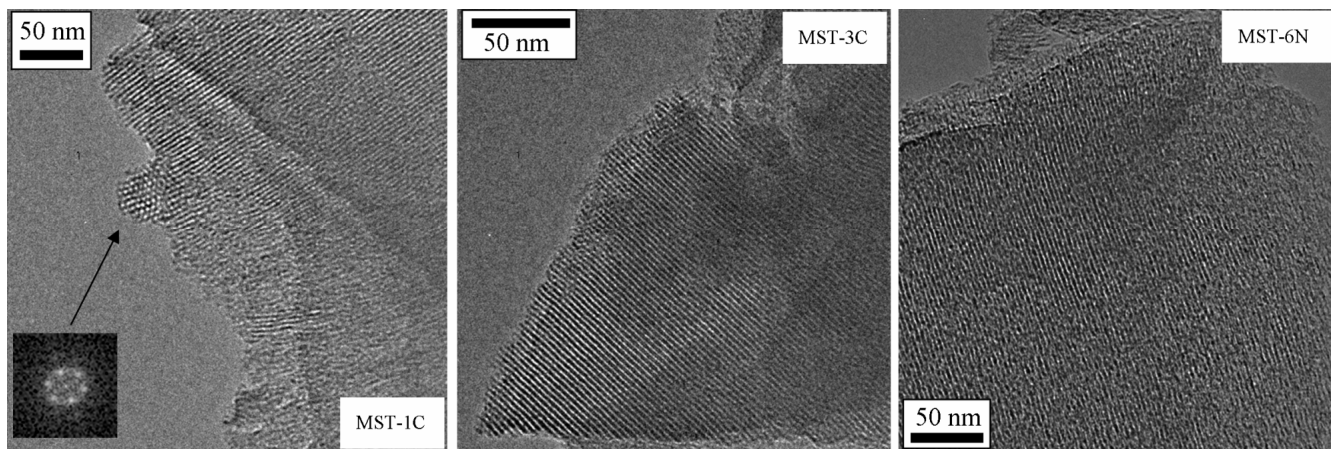


Figure 5. Representative transmission electron micrographs of MST series samples after calcination. The inset is a Fourier transform of the indicated region.

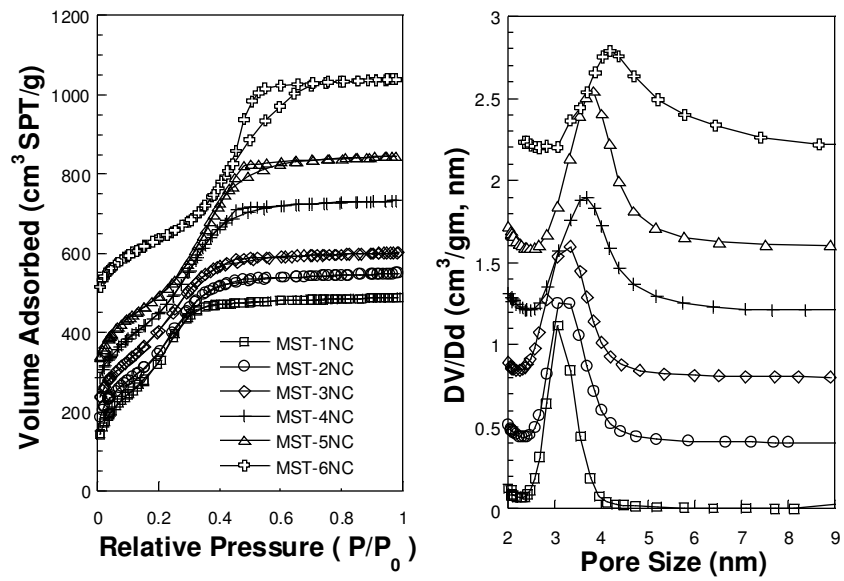


Figure 6. (L) Nitrogen adsorption isotherms and (R) KJS pore size distributions of calcined MST-#NC samples after ammonia treatment.

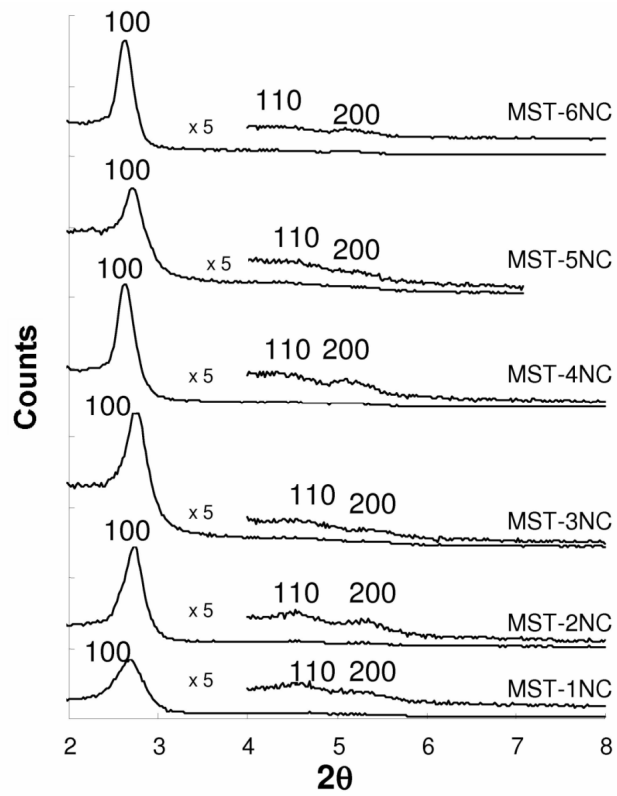


Figure 7. XRD patterns for series MST-#NC samples after ammonia treatment and calcination.

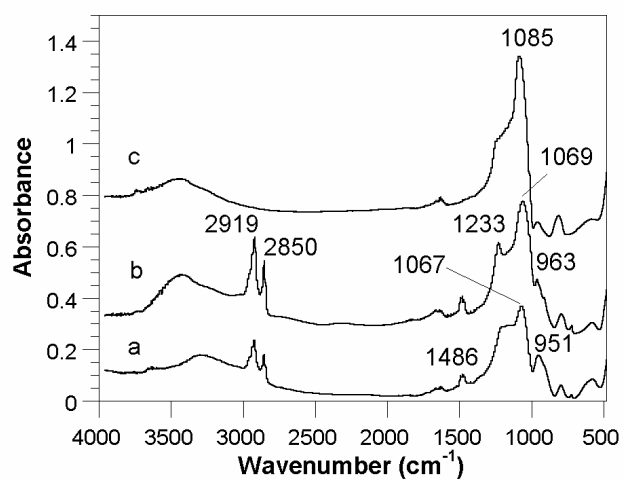


Figure 8. FTIR spectra for one representative mixed surfactant composition (1 g CTAB : 0.2 g C₈G₁) (a) as-made material before ammonia treatment, (b) as-made material after ammonia treatment, and (c) mesoporous silica material after calcination.

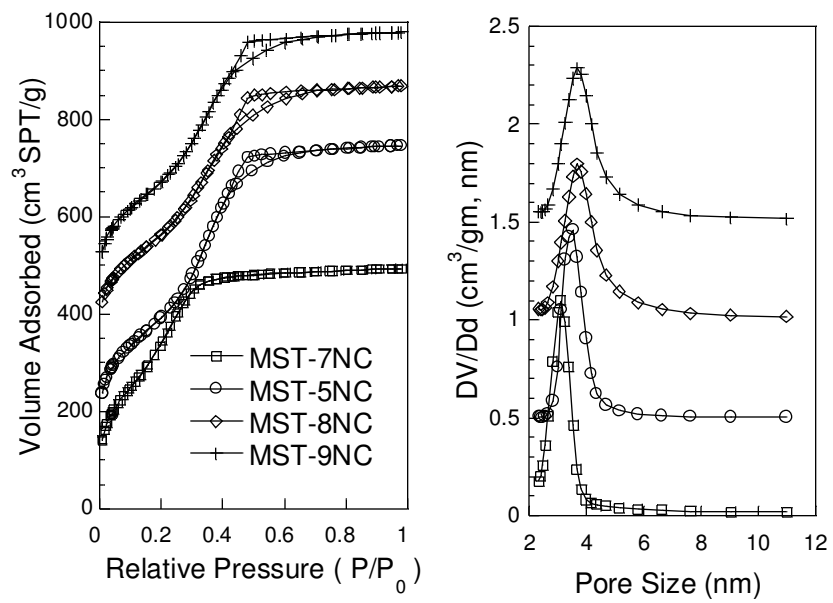


Figure 9. (L) Nitrogen adsorption isotherms and (R) KJS pore size distributions for samples treated with different amounts of ammonia (increasing from bottom to top) after calcination.

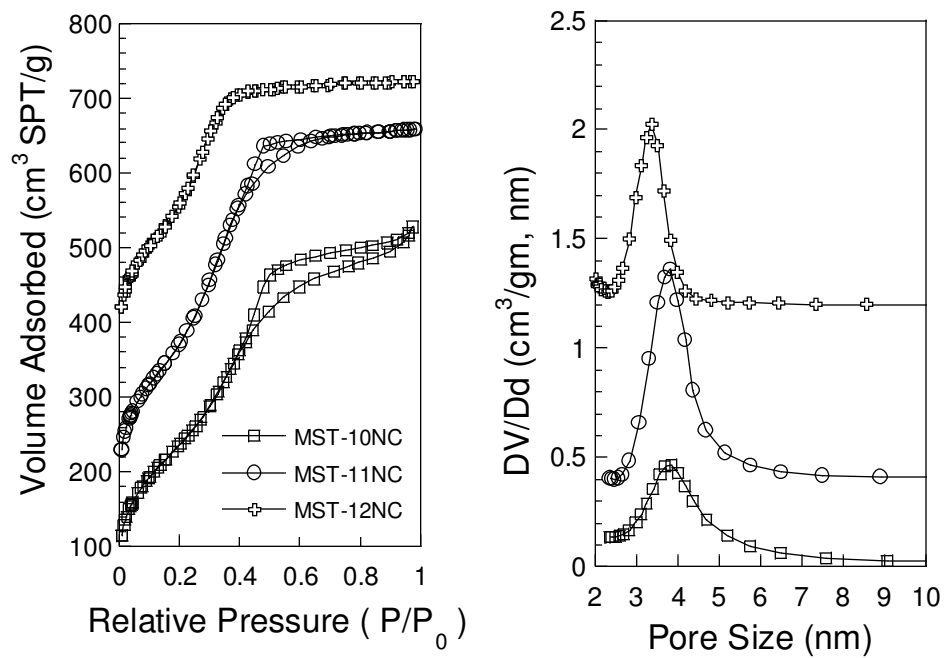


Figure 10. (L) Nitrogen adsorption isotherms and (R) KJS pore size distributions for samples synthesized with different amount of precursor (increasing from bottom to top).

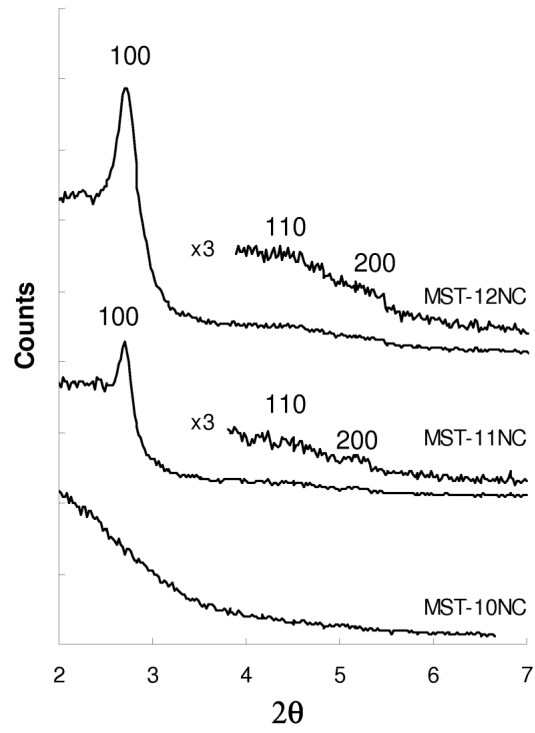


Figure 11. XRD patterns for samples synthesized with different amounts of precursor (increasing from bottom to top).

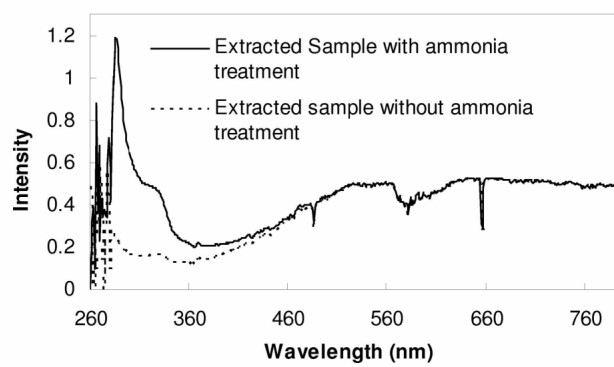


Figure 12. The UV-visible absorbance spectra of ethanol solutions extracted from uncalcined materials prepared with 0.2 g C₈G₁ : 1 g CTAB and with or without ammonia treatment.